◆ Human Brain Mapping 30:3172–3187 (2009) ◆

Probabilistic Topography of Human Corpus Callosum Using Cytoarchitectural Parcellation and High Angular Resolution Diffusion Imaging Tractography

Yi-Ping Chao,[1] Kuan-Hung Cho,[1] Chun-Hung Yeh,[2] Kun-Hsien Chou,[3] Jyh-Horng Chen,[1]* and Ching-Po Lin[2,4,5]*

[1]*Interdisciplinary MRI/MRS Laboratory, Department of Electrical Engineering, National Taiwan University, Taipei, Taiwan*
[2]*Department of Biomedical Imaging and Radiological Sciences, National Yang-Ming University, Taipei, Taiwan*
[3]*Institute of Biomedical Engineering, National Yang-Ming University, Taipei, Taiwan*
[4]*Laboratory for Brain Connectivity, Institute of Neuroscience, National Yang-Ming University, Taipei, Taiwan*
[5]*MRI Research Center, National Yang-Ming University, Taipei, Taiwan*

Abstract: The function of the corpus callosum (CC) is to distribute perceptual, motor, cognitive, learned, and voluntary information between the two hemispheres of the brain. Accurate parcellation of the CC according to fiber composition and fiber connection is of upmost important. In this work, population-based probabilistic connection topographies of the CC, in the standard Montreal Neurological Institute (MNI) space, are estimated by incorporating anatomical cytoarchitectural parcellation with high angular resolution diffusion imaging (HARDI) tractography. First, callosal fibers are extracted using multiple fiber assignment by continuous tracking algorithm based on q-ball imaging (QBI), on 12 healthy and young subjects. Then, the fiber tracts are aligned in the standard MNI coordinate system based on a tract-based transformation scheme. Next, twenty-eight Brodmann's areas on the surface of cortical cortex are registered to the MNI space to parcellate the aligned callosal fibers. Finally, the population-based topological subdivisions of the midsagittal CC to each cortical target are then mapped. And the resulting subdivisions of the CC that connect to the frontal and somatosensory associated cortex are also showed. To our knowledge, it is the first topographic subdivisions of the CC done using HARDI tractography and cytoarchitectonic information. In conclusion, this sophisticated topography of the CC may serve as a landmark to further understand the correlations between the CC, brain intercommunication, and functional cytoarchitectures. *Hum Brain Mapp 30:3172–3187, 2009.* **© 2009 Wiley-Liss, Inc.**

Key words: corpus callosum; parcellation; high angular resolution diffusion imaging; tractography; Brodmann's areas

Contract grant sponsor: National Science Council, Taiwan; Contract grant numbers: NSC-96-2627-B-010-010, NSC-97-2752-H-010-004-PAE. Thanks to Maxime Descoteaux who provided lots of suggestions for this paper.

*Correspondence to: Jyh-Horng Chen, PhD, Department of Electrical Engineering, National Taiwan University, No. 1, Sec. 4, Roosevelt Road, Taipei, Taiwan. E-mail: jyhhchen@gmail.com or Ching-Po Lin, PhD, Institute of Neuroscience, National Yang-Ming University, 155 Li-Nong St., Sec. 2, Taipei 112, Taiwan. E-mail: cplin@ym.edu.tw

Received for publication 8 September 2008; Revised 22 December 2008; Accepted 31 December 2008

DOI: 10.1002/hbm.20739
Published online 24 February 2009 in Wiley InterScience (www.interscience.wiley.com).

INTRODUCTION

Corpus callosum (CC), containing more than 300 million axons, is the major interhemispheric commissure that connects most of the cortical areas in the brain and is responsible for integrating the sensory, cognitive, motor, and learned information between two cerebral hemispheres. According to the topological model of [Clarke and Zaidel, 1994; Witelson, 1989], callosal fibers enter the CC from homologous cortical areas and course medially in a compact bundle, terminating in the opposite hemisphere, as well as in heterotypical areas. Using magnetic resonance imaging (MRI), the relationship between the architecture of CC and neural pathology has been extensively studied and described in the literature, showing that callosal morphology at the midsagittal region is related to dyslexia [Hynd et al., 1995], schizophrenia [Brambilla et al., 2005; Miyata et al., 2007; Narr et al., 2000, 2002; Randall, 1983], Williams syndrome [Luders et al., 2007; Tomaiuolo et al., 2002], attention-deficit hyperactivity disorder (ADHD) [Giedd et al., 1994; Semrud-Clikeman et al., 1994; Skranes et al., 2007], and bimanual function [Meyer et al., 1998; Muetzel et al., 2008]. Therefore, accurate characterization of the callosal fibers is of upmost important.

Because of the fact that there are no characteristic landmarks by which the midsagittal structural and functional callosal-subdivisions can be identified, numerous approaches have been proposed to subdivide the CC into several geometric partitions, including sectioning the CC according to its specific fractions of the maximal anterior–posterior length [Duara et al., 1991; Witelson, 1989], particular angular rays from the callosal centroid [Weis et al., 1993], and several rays normal to a series of equidistant nodes on the ventral callosal boundary [Clarke and Zaidel, 1994; Rajapakse et al., 1996; Stievenart et al., 1997]. However, it should be noted that these geometric partitioning methods are neither based on fiber composition of the CC nor on the fiber connection through the CC. The use of various partitioning methods may lead to the discrepancies between study results on gender, handedness, and schizophrenia related to the CC areas [Diwadkar et al., 2004; Westerhausen et al., 2004].

Development of diffusion tensor magnetic resonance imaging (DT-MRI) has provided a unique approach for noninvasively gathering information regarding microstructures of white matter [Basser et al., 2000]. This technique reveals the major orientation of fiber tracts by measuring molecular diffusivity of water within fibrous brain tissue. The first eigenvector of the tensor model and the corresponding streamline-based tractography algorithms have been employed to reveal white matter pathways within the brain, including cortical spinal tracts, fronto-occipital fasciculus, arcuate fasciculus and superior longitudinal fasciculus [Catani et al., 2005; Makris et al., 2007; Wakana et al., 2004]. Furthermore, distinct tissues such as the thalamus, Brodmann's area (BA) 44/45 and SMA/pre-SMA, Broca's area and internal capsule, have been parcellated by utilizing underlying white matter pathways [Anwander et al., 2007; Johansen-Berg et al., 2005; Klein et al., 2007; Zarei et al., 2007]. Therefore, in vivo examination of the CC fiber connectivity and subdivisions of the CC can be conduced using DT-MRI as well as cortical parcellation [Abe et al., 2004; Cook et al., 2005; Dougherty et al., 2005; Hofer and Frahm, 2006; Huang et al., 2005; Park et al., 2008; Styner et al., 2005; Wahl et al., 2007; Zarei et al., 2006]. Furthermore, the CC fiber properties of the subdivisions have consequently been evaluated using diffusion quantitative indices, such as fractional anisotropy (FA) and mean apparent diffusion coefficients (ADCs) [Chepuri et al., 2002; Hofer and Frahm, 2006].

However, most existing studies parcellate the CC in only six or seven partitions merely according to their empirical definitions of target ROIs placed close to the cortex, which might lead to the incongruous results of the CC subdivisions. Among these studies, Park et al. proposed the only cortical parcellation scheme that included ~47 cortical subregions according to geometric features using outer anatomical landmarks determined by T1 images, even though not based on cytoarchitecture [Park et al., 2008].

We propose to improve current topographic subdivisions of the CC by the following 2 contributions: (1) include cytoarchitectonic information and (2) perform high angular resolution diffusion imaging (HARDI) tractography. BAs were originally defined and numbered by Korbinian Brodmann in the most widely used reference map of the brain. It was constructed as a cytoarchitectonic map based on differences in cell layers and structures, but the areas turned out in general to correspond to different psychological functions [Brodmann, 1909]. The benefit of subdivisions based on cytoarchitectonics is to provide elaborated parcellation of the cortex that should lead to further parcellation of the CC, increasing the amount of anatomical information within the CC [Huang et al., 2005]. For example, the wide range of the CC, which is occupied by fiber interconnecting the superior frontal cortex, could further be subdivided if the cytoarchitectonics-based subdivisions were used [Park et al., 2008].

Moreover, due to the inherent limitations of the diffusion tensor model in describing neural heterogeneity [Tuch et al., 2002], it is difficult to resolve neural projections from the CC toward the lateral and the inferior brain regions where contain crossing fibers, such as the intersection of internal capsule fibers and inferior longitudinal fascicles [Hofer and Frahm, 2006; Park et al., 2008]. Such fiber crossing problem may consequently result in failure to reveal primary diffusion direction and thus increase the uncertainty in fiber tracking as well as further the mapping of CC topography.

HARDI has been proposed for resolving heterogeneity of white matter fibers within an MR voxel [Tuch et al., 2002]. By using the multitensor approach or solving the diffusion orientation distribution function (ODF) of multiple fiber structures within a voxel, these methods of

HARDI successfully elucidated well-known white matter tracts and tract intersections [Alexander, 2005; Ozarslan et al., 2006; Tournier et al., 2004; Tuch, 2004; Tuch et al., 2002, 2003; Wedeen et al., 2005]. Also, complementing tractography algorithms for multiple fiber tracking have been implemented to demonstrate the feasibility of describing complex fiber architecture and to exhibit anatomical connections in areas of complex fiber orientations [Behrens et al., 2007; Berman et al., 2008; Campbell et al., 2005; Chao et al., 2007, 2008a; Descoteaux et al., 2008; Iturria-Medina et al., 2007; Morris et al., 2008; Parker and Alexander, 2005; Pichon et al., 2005; Savadjiev et al., 2006, 2008; Zhang et al., 2008].

The aim of this study was to incorporate two techniques, HARDI-based tractography and anatomical cytoarchitecture parcellation, to estimate detailed population connectivity maps of the midsagittal section of the CC in the standard MNI space. q-ball imaging (QBI) [Tuch, 2004], one of the HARDI methods, was applied to directly derive the ODF from diffusion images using the spherical harmonic q-ball reconstruction approach [Descoteaux et al., 2007; Hess et al., 2006]. QBI can discriminate multiple fiber populations such as the neuronal projections toward to temporal lobe [Descoteaux et al., 2008]. In this group study, callosal fibers of 12 healthy subjects were extracted with the multiple fiber assignment by continuous tracking (MFACT) algorithm [Chao et al., 2008a], which showed success in tracking through complex regions of fiber crossing, such as the well-known fiber tract dispersions from the internal capsule, cortical spinal tracts, and fornix. These fibers were further coregistered to the Montreal Neurological Institute (MNI) space using a tract-based transformation scheme [Chao et al., 2008b]. The transferred fibers were then semiautomatically labeled according to their connection to the precise cortical regions derived from BAs template [Brodmann, 1909; Thottakara et al., 2006], which included ~28 selected subregions located at the surface of the cortical areas. After classifying the transcallosal fibers according to their cortical cytoarchitecture projections in all subjects, topological population connection maps of the CC parcellation were presented in the MNI coordinate system.

METHODS

Subjects

Twelve healthy volunteers (19–26 years of age; seven females) participated in this study. All subjects were right-handed and none had any history of brain injury, epilepsy, or neurological abnormality. Each subject was completely informed regarding the study prior to MRI examination by a research physician and signed the informed consent form. The study was conducted under the guidelines for use of human subjects, approved by the institutional review board at National Yang-Ming University, Taipei, Taiwan.

Image Acquisition

MRI data from human subjects was acquired using a GE Healthcare Signa 1.5T Excite scanner (General Electric, Milwaukee, WI) with an eight-channel head coil. To reduce artifacts caused by motion during the scan, the subject's head was immobilized inside the coil with foam cushions. A three-dimensional fluid-attenuated inversion-recovery fast spoiled gradient recalled echo (FLAIR-FSPGR) was performed to obtain 124 continuous high resolution T1-weighted anatomical images (T1WI), covering the whole brain. The images were acquired parallel to the anterior commissure–posterior commissure line. The imaging parameters were the following: TR = 8.548 ms, TE = 1.836 ms, TI = 400 ms, flip angle = 15°, field of view (FOV) = 256 × 256 mm^2, matrix size = 256 × 256, without gaps, yielding the in-plane resolution of 1 mm^2, and the slice thickness = 1.5 mm.

QBI was performed along the same anatomical direction as the T1 images using a single-shot diffusion spin-echo echo planar imaging (EPI) sequence with TR = 17,000 ms, TE = 91.2 ms, FOV = 256 × 256 mm^2, matrix size = 128 × 128, yielding voxel size = 2 × 2 × 2.2 mm^3. To cover the entire cerebrum, 46 transverse sections were acquired. One hundred and sixty-two diffusion-weighted images (four-fold-tessellated icosahedrons) [Cho et al., 2008; Tuch, 2004] with b value of 3,000 s/mm^2 and one reference (b = 0) were acquired. The total time for both T1WI and diffusion scans was around 60 minutes.

Tracts Extraction

The registration function of Statistical Parametric Mapping 2 (SPM2, Wellcome Department of Cognitive Neurology, London, UK) was employed for motion correction of the diffusion images. With this algorithm, the diffusion-weighted images were aligned with the $b = 0$ image by the mutual information cost function, thus reducing spatial distortion. QBI was utilized in this study to visualize populations of multiple fibers and to reveal the crossing-fibers within neural architecture. Instead of interpolating data points using radial basis function [Tuch, 2004], the spherical harmonic q-ball reconstruction was applied to estimate fiber ODFs [Descoteaux et al., 2007; Hess et al., 2006], which is analytical, fast, more robust to noise and requires less DWI measurements to obtain a good angular resolution. The ODFs were derived from the spherical harmonic QBI with harmonic series order = 12 and were displayed by surface rendering of 320 triangles. Finally, fiber orientations were determined by estimating the local maximum of ODF in 3D space [Cho et al., 2008]. The primary orientations of each ODF were selected by deleting the two less peak values in each triangle repeatedly. Computation was done with an in-house Matlab program (MATLAB 7, Mathworks, USA) that took about 48 minutes per QBI dataset.

Fiber tracking was performed using the MFACT algorithm with a length threshold of ODF (ODF_{td}) 0.8 and a

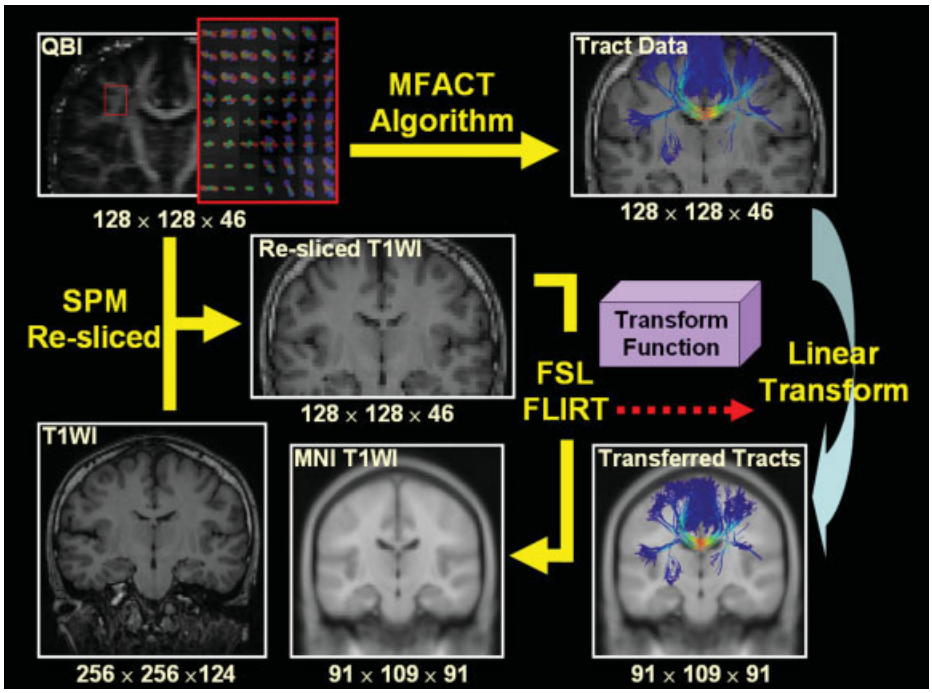

Figure 1.

Flowchart of the tract-based transformation. Fiber tracts reconstructed from individual native space are transformed to the standard MNI coordinate system using the spatial transformation function, which was derived from registration between the resliced TIWI and the ICBM-152 T1WI. This allowed for group analysis of the CC topography derived from cytoarchitectural parcellation. The tracts are color-coded according to the distance between seed point and target voxel. [Color figure can be viewed in the online issue, which is available at www.interscience.wiley.com.]

tract-turning angle threshold (TTA) of 45°. These two thresholds have been proven in previous research [Chao et al., 2008a], and the tracking results were consistent with known anatomy and demonstrated the promising potential in mapping the complex neuronal architecture in the human brain. Moreover, two previously established methods were used for tracing the fiber trajectories: (1) the multiple regions of interest (ROIs) [Mori and van Zijl, 2002] and (2) the brute-force methods [Huang et al., 2004]. All fiber tracts were reconstructed using an in-house program, developed with Borland C++ Builder 6 (Borland, USA).

Tracts Transformation

To evaluate the subdivision of CC and to estimate the probabilistic topography of CC from all subjects, it was important to normalize the reconstructed tracts of all subjects from individual spaces to a common space. The MNI coordinate system (ICBM-152 template) was used [Mazziotta et al., 1995]. A tract-based transformation approach was employed to transfer the extracted tracts from each subject into the MNI coordinate system [Chao et al., 2008b]. To achieve this transformation, we first coregistered and resliced with SPM2, the T1WI with respect to the reference diffusion images. By doing so, the coregistered and resliced T1WI were in the same coordinate system as the tract data. The coregistered and resliced T1WI (DWI space) was used as the input image for each subject to obtain the transformation matrices from individual space to the MNI space. We then extracted the callosal fibers that passed through both the selected ROIs in a midsagittal cross-sectional image of the CC and the BAs from these normalized tract data. The extracted tracts from individual subjects were mapped to the MNI coordinate system using the generated transformation matrices. The flowchart of the tract-based transformation is shown in Figure 1.

Extraction of Callosal Fiber Bundles

To identify callosal fibers in individual and in group templates for population-based topography, ROIs in the individual space and in the MNI space were selected. In the individual space, tracking seed points were assigned in the midsagittal planes of the CC. For avoiding the error of coregistration between individual coordinate and the MNI coordinate, CC shapes were outlined from the eight midsagittal planes by two experienced physicians to cover the CC center of the resliced T1 anatomy images. From

selected CC voxels of individual subjects, around 1,400 seed voxels, were used to compute the complex neural tracts with crossing and branching using the MFACT algorithm [Chao et al., 2008a]. All the extracted tracts were then transferred by tract-based transformation for further clustering of the callosal fibers. To filter out the erroneous tracts generated by the tract-based transformation or manual definition of the ROIs of CC in individual spaces, contours of the CC in ICBM-152 template were used to reject fibers outside of the CC. This refined callosal fiber bundles passing through the contours of the CC in MNI coordinate system.

Clustering of Corpus Callosal Fibers Using Cytoarchitectonic Subdivisions

To achieve a reliable identification of fiber bundles, these tracts were clustered and labeled using the cytoarchitectonic subdivisions derived from the BAs template provided with MRIcro (MRIcro, software by C. Rorden; http://www.sph.sc.edu/comd/rorden/mricro.html), which has been applied as ROI selection to study white matter tractography previously [Thottakara et al., 2006]. This template provides the 40 significant brain subregions according to their functionality and cytoarchitecture by excluding regions belong to monkeys (BAs 13–16, 27, and 49–51). From the 40 subregions, 28 subregions (BAs 1–11, 17–22, and 37–47) were selected by excluding the internal layers (BAs 12, 23–26, 28–36, 48, and 52). The callosal fiber bundles were then classified into 28 subdivisions according to the cortical areas that the fiber branches connected.

Probabilistic Topography of the CC

With QBI and the MFACT algorithm, reconstructed fiber bundles from a single CC seed voxel can terminate in several cortical regions. Therefore, for each subject, each CC voxel had connection probabilities to different cortical regions. Two of the most primary connections of each CC voxel were obtained for further evaluation (see Appendix). For group analysis, a population-based probabilistic connection map to a specific BA was created using Park's approach [Park et al., 2008]. For each CC voxel, the connection probability was defined as the follows:

$$P(v,b) = \frac{1}{S}\sum_{s=1}^{S} \rho(s,v,b) \quad (1)$$

where $P(v, b)$ was the population-based connection probability of the voxel v connected to a selected BA b (b is a serial number of the 28 selected BAs) of all subjects (S = 12). $\rho(s, v, b)$ was a Boolean function that was assigned to be 1 for each single subject if a callosal fiber connected from a voxel v to a selected BA b. Finally, CC voxel probabilities in the resulting group maps for each BA reflect the ratio of the number of subjects who show dominant connections between CC voxels and the cortical BA of interest.

RESULTS

Callosal fiber tracts from seed voxels within an identified region of the CC were extracted from each individual subject using QBI and the MFACT algorithm. The tracking pathways connected into the cortical regions from selected CC regions, as Tuch reported [Tuch, 2004; Tuch et al., 2003]. Figure 2a presents a sagittal view of a 3D reconstruction of callosal fibers projecting into different cortical regions with a background image of resliced T1WI. The lateral and the inferior projections from the CC were clearly revealed, even though connections passed through some areas with intravoxel heterogeneity (e.g., the centrum semiovale). After coregistering to ICBM-152 template using a tract-based transformation, callosal fiber tracts were transformed from their native space into the standard MNI coordinate system for further group analysis (Fig. 2b). In Figure 2c, a precise brain region in the MNI space was defined and presented as an example of extracted callosal fibers that connect to the BA 4 (primary motor cortex). Note that several tracts project to the lateral cortex in this example (even though the majority goes to the vertices of cortex). Callosal fibers were further categorized according to the BAs that they connect, and corresponding CC regions were clustered for group analysis. Figure 3 presents an example of the callosal fibers projected to the temporal regions (BAs 20–22, 37, 38, 41, and 42) and the lateral regions (BAs 43 and 39) of human brain respectively in a single subject. Using QBI and MFACT, callosal bundles were not only observed throughout the vertex of the brain but also the temporal and lateral regions.

Twelve healthy subjects were recruited for this study and a total 28 BAs were located on the cortical surface. To understand the varieties from each subject, the extracted callosal fibers connected to BA 37 (occipito-temporal area) from all subjects were overlaid onto the ICBM-152 template in the MNI space. In spite of the existence of some differences in tracts between each subject, the regions at the CC that neuronal axons passed though were almost located in the splenium (see Fig. 4). In Figure 5, probabilistic topography of the CC as defined by Eq. 1, clearly showed population-based connection maps between the CC and BAs. The selected 28 BAs were clustered by cortical classifications definitions [Hofer and Frahm, 2006], which were demonstrated at the surface of the ICBM-152 template. Cortical clusters of the 28 BAs were the frontal lobe (BAs 8–11 and 44–47), the premotor and supplementary motor areas (BA 6), the primary motor cortex (BA 4), the primary sensory cortex (BAs 1–3 and 5), the parietal lobe (BAs 7, 39, 40), the occipital lobe (BAs 17–19), the temporal lobe (BAs 20–22, 37, 38, 41, and 42), and the undefined area (BA 43). Note that BAs 41 and 42 were merged together to be regarded as a cortical target due to

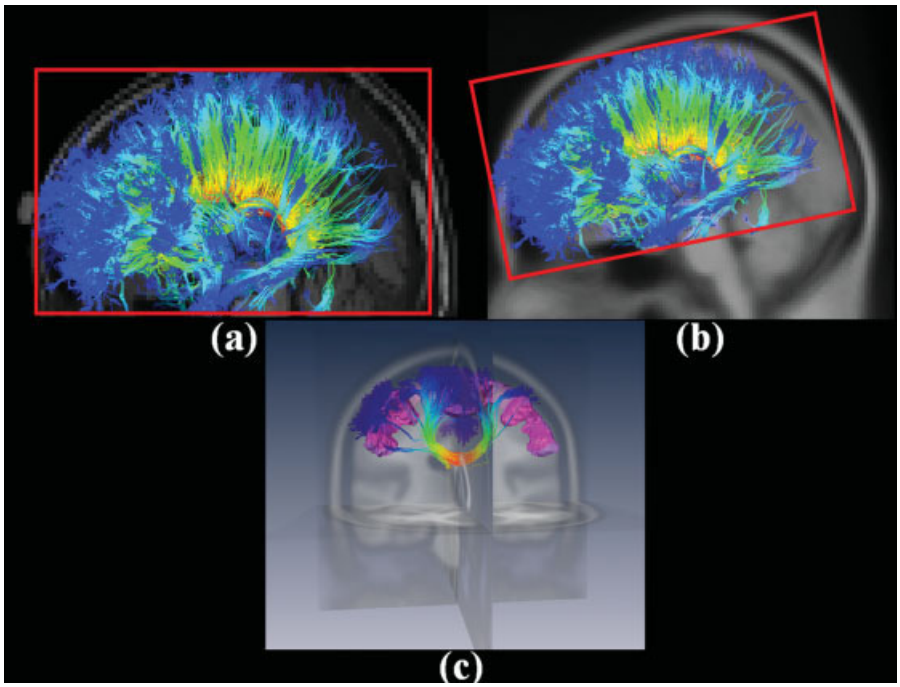

Figure 2.

Callosal fibers of a single subject. (**a**) Callosal fibers extracted by MFACT with QBI overlaid onto the individual's anatomical image (T1WI). (**b**) The spatial normalized callosal fibers superimposed on the ICBM-152 T1 image. The red rectangles in (a,b) show the homologous spatial relationship between individual native space and the MNI coordinate. The neural connections were well preserved after the tract-based transformation. (**c**) An example of the neural connections between the CC and BA, showing the transformed callosal fibers projecting into the primary motor cortex (BA 4). [Color figure can be viewed in the online issue, which is available at www.interscience.wiley.com.]

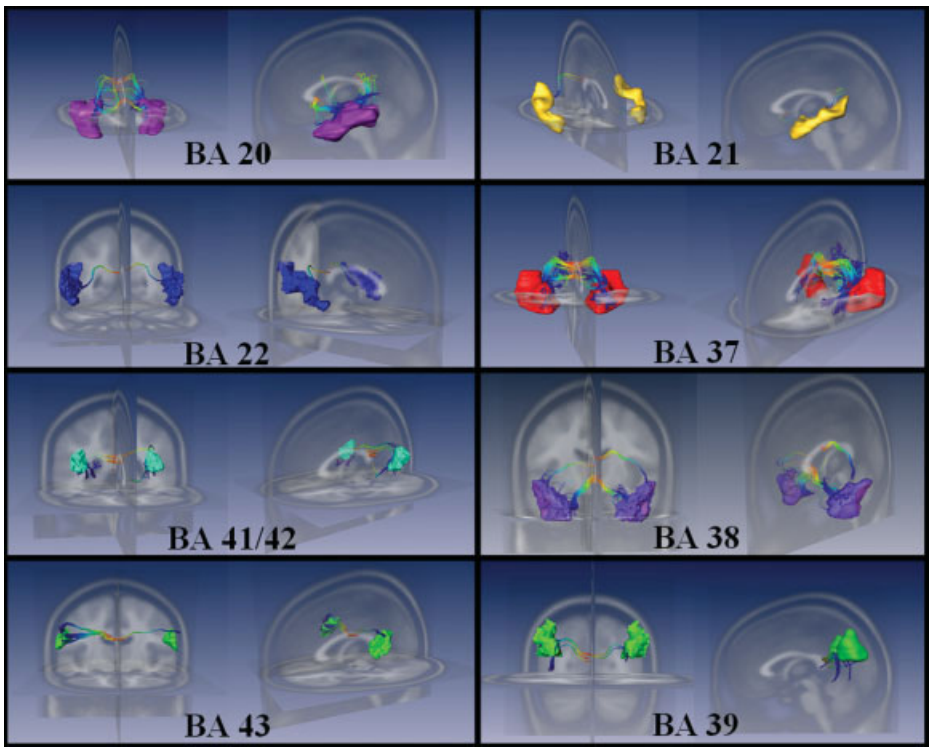

Figure 3.

Three-dimensional (3D) callosal connections projecting to lateral and inferior BAs. Fiber pathways were clustered according to their projecting targets, temporal lobes (BAs 20–22, 37, 38, and 41/42) and the lateral regions (BAs 43 and 39) of human brain respectively in a single subject. Integrating QBI and MFACT algorithm, fiber tracts between the CC and temporal as well as lateral regions can be identified. [Color figure can be viewed in the online issue, which is available at www.interscience.wiley.com.]

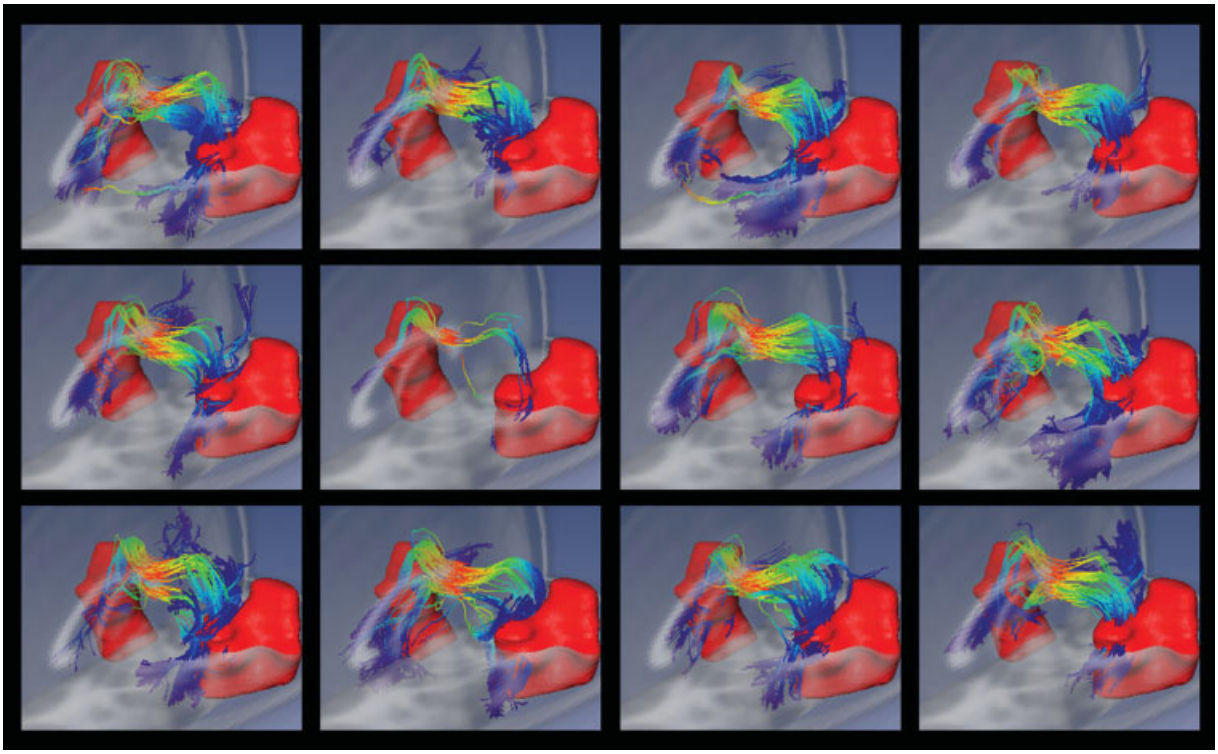

Figure 4.
Callosal fibers connected to BA 37 (occipito-temporal area) were overlaid on the ICBM-152 T1 image in the MNI coordinate. The tracts are consistent between all subjects ($n = 12$). [Color figure can be viewed in the online issue, which is available at www.interscience.wiley.com.]

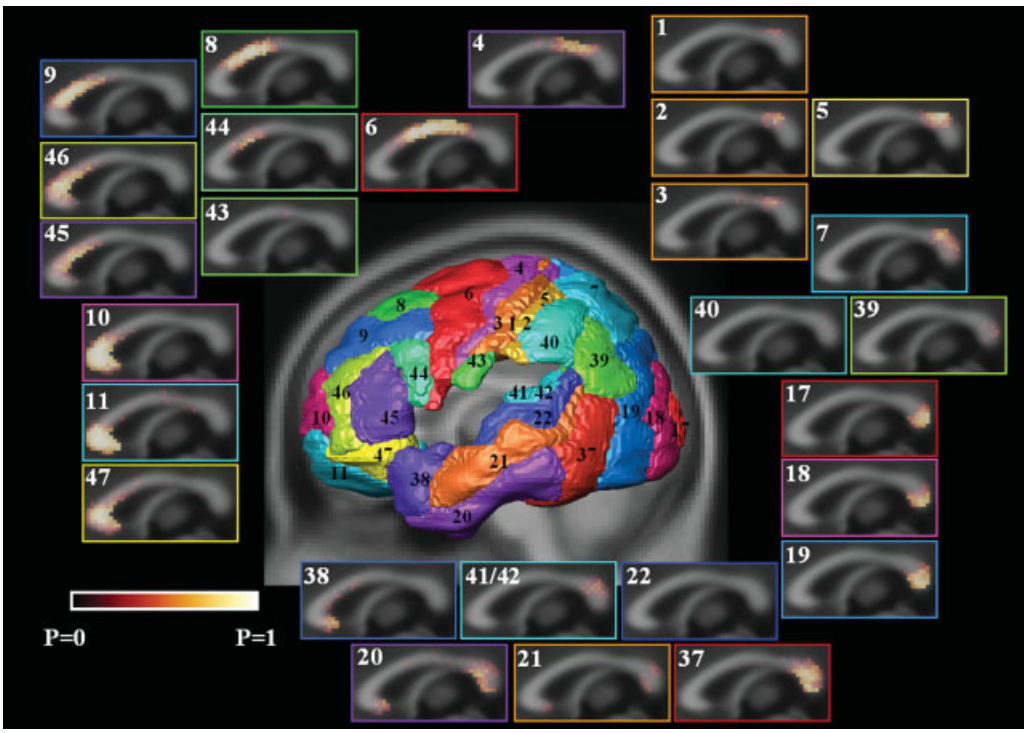

Figure 5.
Probabilistic topography of the midsagittal CC. Twenty-eight BAs located at the surface of the cerebrum were considered as the terminal regions for cytoarchitecture parcellation. The CC was partitioned into subdivisions based on their commissural connections to the corresponding BAs, and then a population-based probability topography of CC was constructed from 12 subjects. The color scale shown at the left bottom represents the population probability of a given voxel within the CC projecting to a particular BA. [Color figure can be viewed in the online issue, which is available at www.interscience.wiley.com.]

TABLE I. Topographic connection distributions of the CC by connectivity projecting to specific cortical regions

Cortical region	Brodmann's area	Major connection distribution in corpus callosum
Frontal lope	BA 8	Rostral body and anterior midbody
	BA 9	Genu, rostral body, and anterior midbody
	BA 10	Rostrum, genu, and rostral body
	BA 11	Rostrum and genu
	BA 44	Ventral rostral body and ventral anterior midbody
	BA 45	Genu, rostrum, rostral body, and anterior midbody
	BA 46	Genu, rostrum, rostral body, and anterior midbody
	BA 47	Genu, rostrum, rostral body, and anterior midbody
Premotor and supplementary motor cortex	BA 6	Anterior midbody and posterior midbody
Primary motor cortex	BA 4	Posterior midbody and isthmus
Primary sensory cortex	BA 1	Isthmus
	BA 2	Isthmus
	BA 3	Posterior midbody and isthmus
	BA 5	Isthmus and superior splenium
Parietal lope	BA 7	Dorsal splenium
	BA 39	Dorsal splenium
	BA 40	Dorsal splenium
Occipital lope	BA 17	Posterior splenium
	BA 18	Posterior splenium
	BA 19	Posterior splenium
Temporal lope	BA 20	Rostrum, dorsal splenium, and ventral splenium
	BA 21	Rostrum and splenium
	BA 22	Ventral splenium
	BA 37	Splenium
	BA 38	Genu, rostrum, and ventral rostral body
	BA 41/42	Superior splenium
Other cortical region	BA 43	Posterior midbody

their similar function and smaller volume that fewer callosal pathways connect.

Probabilistic topography of the CC showed the principal distribution of fiber projections that interconnected with the related BAs. A higher probability in the topography was indicative of callosal connections passing through the CC voxel corresponding to the BA valid for the majority. All these connections are reported in Table I, and we now enumerate our observations in the following. (1) The topography maps show that neuronal pathways projected to the frontal lobe, including the intermediate frontal, the granular frontal, the frontopolar, the prefrontal, the opercular, the triangular, the middle frontal, and the orbital frontal lobe (BAs 8–11 and 44–47), passing through the rostrum, genu, rostral body, and the anterior midbody of the CC. (2) The predominant regions, where fibers interconnected through the premotor and supplementary motor regions (BA 6), were in the anterior midbody and posterior midbody of the CC. (3) Neuronal tracts between the primary motor cortex (BA 4) and the CC mainly passed through the posterior midbody and isthmus of CC. (4) Fibers terminating in the intermediate postcentral, caudal postcentral, rostral postcentral and preparietal (BAs 1–3 and 5) of the primary sensory cortex interconnected via the posterior midbody, isthmus and superior splenium of the CC. (5) The predominant regions of fiber tracts passing through the superior parietal, angular, and supramarginal (BAs 7, 39, and 40) of the parietal lobe were in the upper region of the splenium. (6) Neuronal pathways connected to the occipital lobe, including striate, parastriate and peristriate (BAs 17–19), passed through the posterior region of the splenium. (7) Tracts connected to the temporal lobe, including inferior temporal, middle temporal, superior temporal, occipitotemporal, temporopolar, anterior transverse temporal, and posterior transverse temporal cortex (BAs 20–22, 37, 38, 41, and 42), generally passed through the rostrum, superior and ventral region of the splenium, and the ventral rostral body of the CC. (8) Tracts projecting to the subcentral area (BA 43) passed via the posterior midbody of the CC.

DISCUSSION

The function of the CC is to distribute perceptual, motor, cognitive, learned, and voluntary information between the left and right hemispheres of the brain [Bogen et al., 1965]. Given the importance of sharing sensory, visual and cognitive callosal messages between bilateral hemispheres, it is imperative that this anatomic region has extremely complicated connections between various functional regions of the cerebral cortex. By incorporating HARDI-based tractography and the cytoarchitectonic BAs template, we presented a probabilistic topography of the CC according to their neural connections with distinct cerebral areas. Based on the characters of HARDI tractography, callosal fiber tracts coursed from the CC and propagated through heterogeneous brain regions into various BAs were revealed

noninvasively, including the inferior and lateral regions of human brain where comprising voxels with crossing fibers. The sophisticated CC topography was useful to reveal regional microstructural differences between healthy and patient subjects.

Probabilistic Topography of the CC

A topography of callosal fibers was specified in 1989 by Witelson [Witelson, 1989]. Pathologic studies have shown that the fibers passing through different regions of the CC serve different functions; varying fractions of these fibers connect heterologous areas of cortex [Brambilla et al., 2004]. Numerous studies based on DTI tractography further distinguished topological partitions of the CC by incorporating callosal parcellation with various ROI selection schemes, such as brief definition of cortical areas [Hofer and Frahm, 2006; Huang et al., 2005; Zarei et al., 2006] or determining geometric features of outer anatomical landmarks by structural MRI [Park et al., 2008]. Here, we clustered the CC subdivisions by parcellating neural pathways that connect the CC and distinct BAs to avoid the discrepancies caused by the various ROI selection schemes among these studies. From the 52 areas defined, 28 were applied in this study. The inner layers and regions found only in monkeys were excluded. Interior BAs were ignored since this study focus on the exterior BAs. Tracts propagation between interior and exterior BAs, and the CC, was not discussed in this study but is worth looking at in the future.

On the other hand, due to the intrinsic limitation of DTI in regions with complex fiber heterogeneity, lateral and inferior projections of the CC may not be resolved well enough by means of DTI-based tractography [Hofer and Frahm, 2006; Huang et al., 2005; Park et al., 2008]. Instead of using DTI, QBI and complex tractography methods were adopted to map the sophisticated callosal trajectories [Berman et al., 2008; Chao et al., 2008a]. With these techniques, there was a higher probability of revealing interhemispheric connections from distinct functional areas. Figures 3 and 4 demonstrated the temporal and lateral callosal pathways propagating from the CC in spite of little tracts astray to orbital frontal lobes (it will be discussed at the last discussion paragraph, *Limitations*). These tracts are normally missed by most DTI-based tracking algorithms. These results of tracking also agree with recently published results from a probability-based HARDI tractography method [Descoteaux et al., 2008].

Figure 5 shows the probabilistic population maps of CC from 28 BAs. It maps a well-ordered topography in relation to each functional unit (Table I). For example, in the frontal cortex, cortical connections from the rostral part of the superior and middle frontal gyrus (BAs 10 and 11) and prefrontal cortex (BAs 46 and 47) interconnect with the rostrum and part of the genu of the CC. Cortical connections from another region of the frontal cortex (BAs 8, 9 and BAs 44, 45) interconnect bilateral hemispheres through the genu and rostral body of the CC. Cortical connections between other BAs also showed well organized topography at the midsagittal CC. When the CC topography is done with larger clustered brain regions, it is consistent with previous reports, even if the temporal and lateral connections are not considered [Zarei et al., 2006]. That is, from the frontal cortex (BAs 8–11 and 44–47), cortical connections mostly passed through the rostrum, genu, and rostral body of the CC. From the premotor cortex (BA 6), primary motor cortex (BA 4) and primary sensory cortex (BAs 1–3 and 5), cortical fibers passed through the midbody, posterior midbody, and isthmus of the CC respectively. Cortical connections at the dorsal and posterior region of the CC splenium terminated at the parietal (BAs 7, 39, and 40) and occipital (BAs 17–19) lobes. Tracts connecting to temporal cortices (BAs 20–22, 37, 41, and 42) occupied a considerable proportion of the splenium.

Subdivisions of Corpus Callosum

Sophisticated subdivisions of the CC on the basis of cortical topography were mapped within this study. It may serve as a brain landmark to reveal the relationship between regional microstructural differences of the CC and diffusion anisotropy indices [Chepuri et al., 2002; Hofer and Frahm, 2006]. And the spatial localization of the CC subdivisions seems to be in well consistence with its associated cortical region. To highlight the subtle regions, Figure 6 shows the complicated subdivisions in accordance to the BAs in frontal lobes and in somatosensory associated cortex. Connecting to frontal lobes, fine topography of the CC was presented (Fig. 6b). The subtle partitions seem to be in agreement with the BA location in frontal lobe, the most important region for the integration of sensory and mnemonic information, the regulation of intellectual function and action, and language function. Such elaborated parcellation of the CC may specify the connections from distinct cortical region and mark the underlying abnormalities of more circumscribed subregions or the associations with psychopathological measure [Miyata et al., 2007] and cognitive performance [Alexander et al., 2007]. It may also facilitate the correlation study between CC subregional abnormalities and psychopathology, such as schizophrenia [Rotarska-Jagiela et al., 2008] and autism [Chung et al., 2004]. In addition, this sophisticated topography of the CC may assist the study of structural and functional organization in human brain, which was previously achieved by integrating functional neuroimages and diffusion tractography [Dougherty et al., 2005; Wahl et al., 2007]. The precise topography of the CC may allow prediction of functional connectivity from variability of microstructure in healthy individuals, and potentially, abnormality of functional connectivity in neurological or psychiatric patients.

Somatosensory associated cortex comprising with primary somatosensory cortex (SI; BAs 1–3) and secondary somatosensory cortex (SII; BA 5) are also similar to their

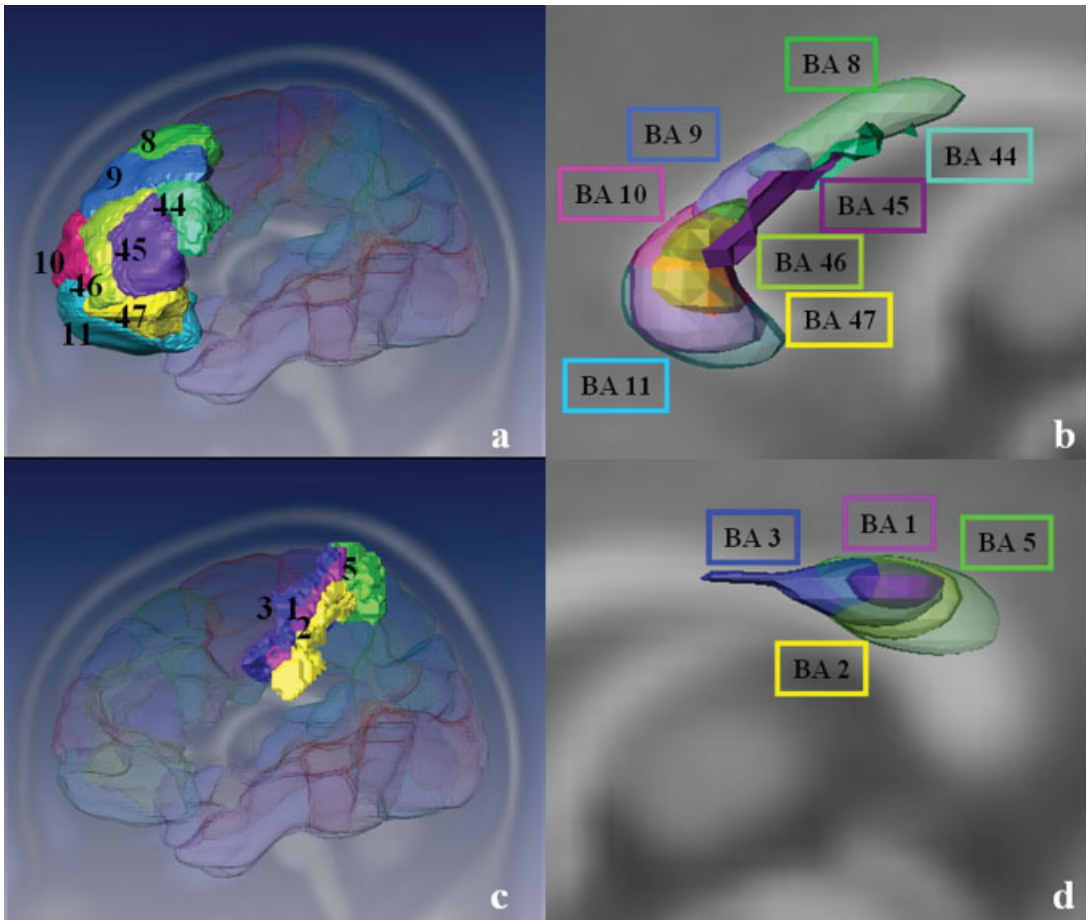

Figure 6.

3D rendering of the sophisticated subdivisions in the CC based on its connections to the frontal and somatosensory associated BAs. Sagittal view of 3D reconstruction of major callosal distributions connected to the selected frontal BAs (BAs 8–11 and 44–47) (**a**) and somatosensory associated cortex (BAs 1–3 and 5) (**c**) were shown by thresholding those voxels in which greater than 50 and 20% of the population probability, respectively (**b** and **d**). Arbitary thresholds were selected to highlight the major callosal distributions based on their complexities and consistencies of tracking pathways. [Color figure can be viewed in the online issue, which is available at www.interscience.wiley.com.]

anterior–posterior extension as well as the topographies of the CC (Fig. 6d). Previous rhesus monkey study has indicated that the projections of the primary somatosensory cortex (BAs 1–3) in the postcentral gyrus has a strong and sequential outflow of connections from area 3 to areas 1 and 2, then from area 1 to area 2 and finally from area 2 to area 5 and rostral area 7 [Vogt and Pandya, 1978]. Although there is no direct evidence from histochemical or classical tracer injection experiment, we suggested that the overlap between these somatosensory subdivisions might be considered the regions with heterogeneous pathways for sharing the interhemispheric transfer of somatosensory information. The presumption could provide an effective clue to indicate that callosal fibers enter the CC from homologous cortical areas and course medially in a compact bundle, terminating in the opposite hemisphere, as well as in heterogeneous areas, for integrating cortico-cortical interhemispheric transfer of information.

Validity of the CC Topography

To further verify the validity of our topographical map, the first primary BA connection to the voxel in midsagittal CC was calculated. Callosal connections projected to 28 defined BAs were reassigned to 7 cortical targets (Fig. 7a), comprising frontal cortex (BAs 8–11 and 44–47), premotor and supplement motor cortex (BA 6), primary motor cortex (BA 4), primary sensory cortex (BAs 1–3 and 5), parietal cortex (BAs 7, 39, and 40), occipital lobe (BAs 17–19) and temporal lobe (BAs 20–22, 37, 38, 41, and 42). Using hard segmentation based on the parcellation of cortical clusters [Hofer and Frahm, 2006], global topography of the

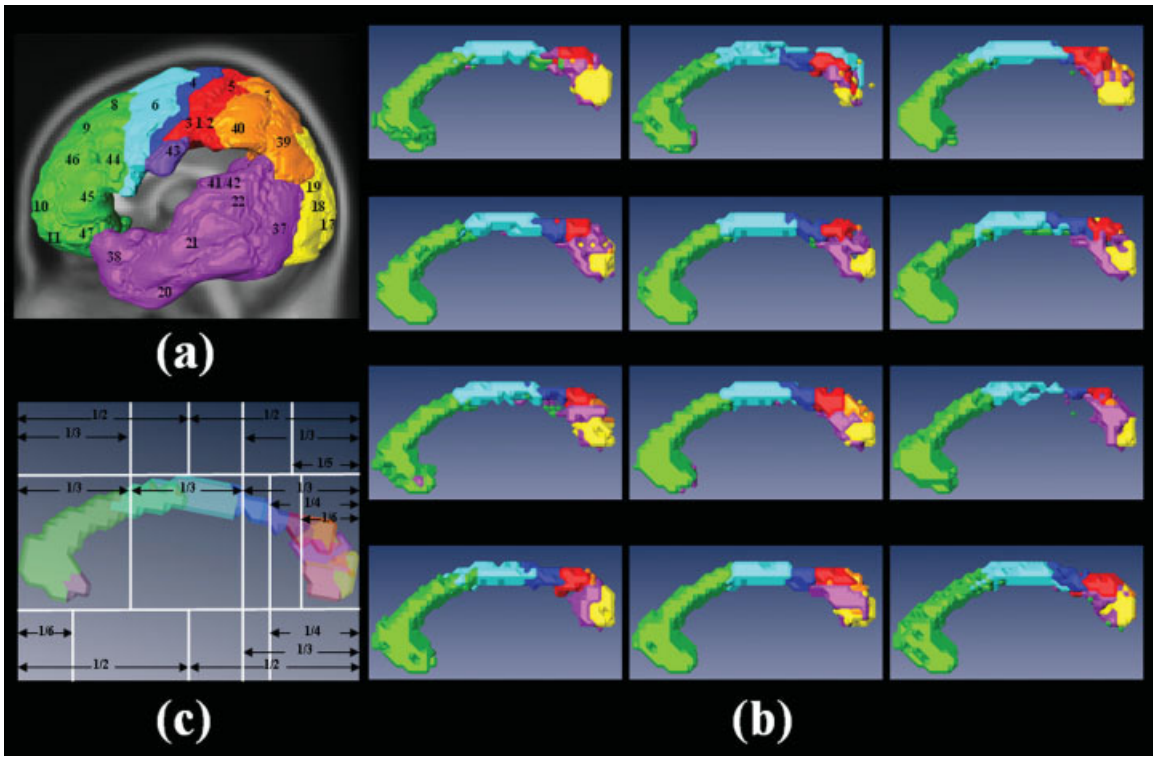

Figure 7.

Hard segmentation of the midsagittal corpus callosum. BAs were reassigned to seven cortical targets, frontal cortex (green), premotor and supplementary motor areas (light blue), primary motor cortex (dark blue), primary sensory cortex (red), parietal lobe (orange), occipital lobe (yellow), and temporal lobe (violet) (**a**). The global topography of each subject was constructed using the hard segmentation method (**b**). In comparison with Witelson's scheme (top), our proposed scheme (middle), and Hofer's scheme (bottom) of the CC classification were shown (**c**). A geometric baseline was defined by connecting the most anterior (left) and posterior (right) points of the CC. According to geometrical baselines defined by Witelson [1989], five vertical partitions of the CC (top) were defined as anterior third (prefrontal, premotor and supplementary motor), anterior midbody (primary motor), posterior midbody (somaesthetic, posterior parietal), isthmus (posterior parietal, superior temporal), and splenium (occipital, inferior temporal). Similar to Witelson, five vertical partitions of the CC (bottom) defined by Hofer and Frahm [2006] were first sixth (prefrontal), the rest of the anterior half of the CC (premotor and supplementary motor), posterior half minus the posterior third (motor), posterior one-third minus posterior one-fourth (sensory), and posterior one-fourth (parietal, temporal and occipital). Our five vertical partitions of the CC (middle) were defined as anterior one-third (frontal), middle one-third (premotor and supplementary motor), posterior one-third minus the posterior one-fourth (motor), posterior one-fourth minus posterior one-sixth (sensory), and posterior one-sixth (parietal, temporal and occipital). [Color figure can be viewed in the online issue, which is available at www.interscience.wiley.com.]

CC from 12 subjects was visualized (Fig. 7b). The results show a high consistency with previous reports [Huang et al., 2005; Zarei et al., 2006] although minor variances in geometric subdivisions of the CC were observed. The subtle discrepancies may be caused by individual differences (compare with the ICBM template) and divergent ROI selection schemes of cortical targets. Another comparison was achieved by label reassigning according to the population-based probabilistic topography of the CC instead of the most dominant BA regions (Fig. 7c). Five vertical partitions of the CC (middle scheme in Fig. 7c) were thus labeled. As shown in Figure 7c, the results are slightly dissimilar to the partitions defined by Witelson [1989] or Hofer and Frahm [2006]. The discrepancies may result from that Witelson's scheme was neither based on the fiber composition of the CC nor on fiber projection to cortical targets and Hofer's scheme was according to the MRI-based subdivision. Such inconsistency between the cytoarchitectonic subdivision and the MRI-based subdivision has been reported in Amunts et al. [2000] and Park et al. [2008]. It is still difficult to evaluate the merits of different classification schemes as there is no large population for comparison. According to functional anatomy or cytoarchitectonic features, population-based probabilistic topography of the CC could be provided with higher reproducibility and reliability than the presentation derived from fiber tracking of an individual [Park et al., 2008; Zarei et al., 2006].

Normalization and Tract-Transformation Problem

Variances between subjects can be presented in a reference space for the further statistical analyses [Huang et al., 2005; Wahl et al., 2007]. For DTI studies, spatial normalization of the diffusion tensor field has been proposed for quantifying group tractography by tensor reorientation approaches [Alexander et al., 2001; Jones et al., 2002; Ming-Chang et al., 2008; Park et al., 2003; Xu et al., 2003; Zhang et al., 2006]. However, these approaches are not applicable to the multiple fiber patterns derived from the HARDI methods as this technique yields complex ODF structures with multiple peaks and indistinct definition of major orientations. To determine CC topography from numerous subjects, a tract-based transformation approach may be applied to process the complex group tractography [Chao et al., 2008b; Hua et al., 2008; Xu et al., 2002]. Using group statistical analysis, the callosal population distribution associated with the functional cortical lobes was calculated. Although tract-based transformation was an efficient method for processing population analysis, the residual variability of gross morphology after spatial normalization may have confounded the parcellation results due to partial volume effect and random noise distribution. Accordingly, probabilistic connection topography was used to provide the interconnection distribution in the midsagittal section of CC to specific BAs. Through statistical calculation across subjects, errors from tract-transformation and individual variance were minimized.

Limitations

Correspondence rates between primary and secondary dominant BA connections from each CC voxel were calculated based on the Eq. 2 and Eq. 3 in Appendix I (Fig. 8a,b). If either the primary or the secondary dominant BA was considered alone, only the genu, anterior midbody and posterior midbody of the CC showed high correspondence rates between 12 subjects. Thus, the primary or secondary callosal connection may be affected by individual variance or the other factors that may vary the accuracy of diffusion tractography (e.g., partial volume effect, signal noise, and tracking criteria, etc). Figure 8c shows the correspondence rate of each CC voxel calculated based on the Eq. 4 to integrate both primary and secondary dominant cytoarchitectonic labels between all individuals. The correspondence rate was highly improved at CC subregions, except the border of CC where the partial volume effect is severe. This result indicates that one primary connection from each CC voxel is not enough to identify the highly condensed commissure as well as the topography distribution of CC. A probabilistic tractography or probabilistic topography is necessary to describe the precise parcellation of cortical subregions.

Several groups have recently used such probabilistic methods [Berman et al., 2008; Campbell et al., 2005; Descoteaux et al., 2008; Morris et al., 2008; Zhang et al., 2008] based on the new fiber ODF (fODF) or the fiber orientation density (FOD) [Tournier et al., 2007] estimation. These methods use the full distribution of the fODF or FOD and thus, similar to DTI probabilistic fiber tracking algorithms [Behrens et al., 2003; Friman et al., 2006; Jones and Pierpaoli, 2005; Lazar and Alexander, 2005; Parker et al., 2003], are more robust to seeding, maxima extraction, noise, and interpolation errors. In this study, by choosing only the most important ODF peaks (>0.8), we are in fact using the principal fiber orientations, which is in a certain way similar to a very sharp FOD. Moreover, similar to the commonly used FACT algorithm for DTI neuroscientific studies, we chose the MFACT algorithm because it is efficient, reproducible, and consistent in practice. Note that it would be possible to extend this MFACT algorithm to obtain probabilistic anatomical connections, using our probabilistic MFACT [Chao et al., 2007] method. This will be part of future investigation.

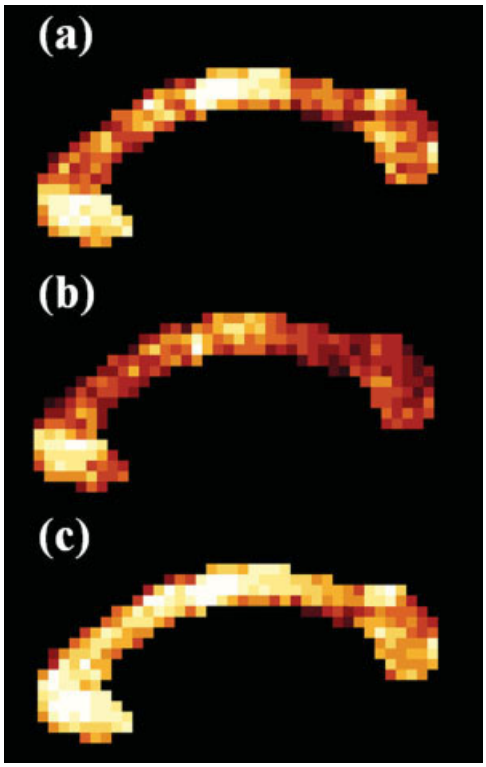

Figure 8.
The correspondence map of the primary (**a**) and the secondary (**b**) dominant BA label of each CC voxel between 12 subjects. The color of each voxel was identical to that of Figure 5. It was obvious that either of the primary or the secondary dominant cytoarchitectural label was not sufficient to show reliability of dominant CC connection map. However, integrating both the primary and secondary most dominant cytoarchitectonic labels resulted in a consistent correspondence map among all individuals (**c**). [Color figure can be viewed in the online issue, which is available at www.interscience.wiley.com.]

Another limitation in this study was the dilemma of excluding tracts and associated commissures for tracts passing through two or more defined BAs to the CC. Such tracts were not excluded in this study since these areas are sometimes geometrically interconnected with each other. From our results, temporal connections from BAs 20, 21, and 38 not only interconnect with the CC splenium but also connect to the genu and rostrum of the CC. It is the only one conflicting result with Zarei et al. [Zarei et al., 2006]. It has been shown that the orbital lobe fibers occupy the rostrum [Huang et al., 2005]. Tracts propagated from BA 38 (temporal polar) to the genu and rostrum of the CC identified in this study may be due to the known connectivity between BA 38 and the orbital frontal lobes (BA 11) [Abe et al., 2004; Petrides and Pandya, 1988]. The same condition occurred at the cortical connections from BA 20 (fusiform gyrus) and BA 21 (superior temporal sulcus). From these areas, temporal fiber connecting to the genu and rostrum of the CC interdigitated with the occipitofrontal fasciculus [Dougherty et al., 2007]. The error may be resolved by further improvements of spatial resolution and diffusion imaging approaches.

CONCLUSIONS

The CC was parcellated based on its cortical trajectories to specific cytoarchitectural regions using HARDI-based tractography and tract-based transformation. Using the HARDI method, we had a greater opportunity than DTI-based approaches to reveal callosal projections through heterogeneous complex brain regions, especially the lateral and the inferior brain regions. From 28 BAs located at the surface of cortical areas, sophisticated probabilistic population topography of the CC from 12 healthy subjects were identified. In comparison with previous results, this study revealed the exquisite subdivisions at the CC based on its connections to distinct brain functional unit. This result promises further understanding of brain intercommunication, fiber compositions in the CC and clinical applications such as corpus callosotomy.

REFERENCES

Abe O, Masutani Y, Aoki S, Yamasue H, Yamada H, Kasai K, Mori H, Hayashi N, Masumoto T, Ohtomo K (2004): Topography of the human corpus callosum using diffusion tensor tractography. J Comput Assist Tomogr 28:533–539.

Alexander DC (2005): Multiple-fiber reconstruction algorithms for diffusion MRI. Ann N Y Acad Sci 1064:113–133.

Alexander DC, Pierpaoli C, Basser PJ, Gee JC (2001): Spatial transformations of diffusion tensor magnetic resonance images. IEEE Trans Med Imaging 20:1131–1139.

Alexander AL, Lee JE, Lazar M, Boudos R, DuBray MB, Oakes TR, Miller JN, Lu J, Jeong EK, McMahon WM, Bigler ED, Lainhart JE (2007): Diffusion tensor imaging of the corpus callosum in Autism. Neuroimage 34:61–73.

Amunts K, Malikovic A, Mohlberg H, Schormann T, Zilles K (2000): Brodmann's areas 17 and 18 brought into stereotaxic space—Where and how variable? Neuroimage 11:66–84.

Anwander A, Tittgemeyer M, von Cramon DY, Friederici AD, Knosche TR (2007): Connectivity-based parcellation of Broca's area. Cereb Cortex 17:816–825.

Basser PJ, Pajevic S, Pierpaoli C, Duda J, Aldroubi A (2000): In vivo fiber tractography using DT-MRI data. Magn Reson Med 44:625–632.

Behrens TE, Johansen-Berg H, Woolrich MW, Smith SM, Wheeler-Kingshott CA, Boulby PA, Barker GJ, Sillery EL, Sheehan K, Ciccarelli O, Thompson AJ, Brady JM, Matthews PM (2003): Non-invasive mapping of connections between human thalamus and cortex using diffusion imaging. Nat Neurosci 6:750–757.

Behrens TE, Berg HJ, Jbabdi S, Rushworth MF, Woolrich MW (2007): Probabilistic diffusion tractography with multiple fibre orientations: What can we gain? Neuroimage 34:144–155.

Berman JI, Chung S, Mukherjee P, Hess CP, Han ET, Henry RG (2008): Probabilistic streamline q-ball tractography using the residual bootstrap. Neuroimage 39:215–222.

Bogen JE, Fisher ED, Vogel PJ (1965): Cerebral commissurotomy. A second case report. JAMA 194:1328–1329.

Brambilla P, Nicoletti M, Sassi RB, Mallinger AG, Frank E, Keshavan MS, Soares JC (2004): Corpus callosum signal intensity in patients with bipolar and unipolar disorder. J Neurol Neurosurg Psychiatry 75:221–225.

Brambilla P, Cerini R, Gasparini A, Versace A, Andreone N, Vittorini E, Barbui C, Pelizza L, Nose M, Barlocco L, Marrella G, Gregis M, Tournikioti K, David AS, Keshavan MS, Tansella M (2005): Investigation of corpus callosum in schizophrenia with diffusion imaging. Schizophr Res 79(2/3):201–210.

Brodmann K (1909): Vergleichende Lokalisationslehre der Grosshirnrinde. Leipzig: Barth.

Campbell JS, Siddiqi K, Rymar VV, Sadikot AF, Pike GB (2005): Flow-based fiber tracking with diffusion tensor and q-ball data: Validation and comparison to principal diffusion direction techniques. Neuroimage 27:725–736.

Catani M, Jones DK, ffytche DH (2005): Perisylvian language networks of the human brain. Ann Neurol 57:8–16.

Chao YP, Yang CY, Cho KH, Yeh CH, Chou KH, Chen JH, Lin CP (2007): Probabilistic anatomical connection derived from QBI with MFACT approach. In: Joint Meeting of the 6th International Symposium on Noninvasive Functional Source Imaging of the Brain and Heart and the International Conference on Functional Biomedical Imaging, 2007. NFSI-ICFBI 2007. IEEE. pp 101–104.

Chao YP, Chen JH, Cho KH, Yeh CH, Chou KH, Lin CP (2008a): A multiple streamline approach to high angular resolution diffusion tractography. Med Eng Phys 30:989–996.

Chao YP, Yeh CH, Chou KH, Cho KH, Chen JH, Lin CP (2008b): Probabilistic tract-based atlas with high angular resolution diffusion imaging. Presented at 16th Scientific Meeting and Exhibition, 3–9 May 2008, Toronto. International Society for Magnetic Resonance in Medicine, 2008. ISMRM 2008. 16th Scientific Meeting and Exhibition Number 1838.

Chepuri NB, Yen YF, Burdette JH, Li H, Moody DM, Maldjian JA (2002): Diffusion anisotropy in the corpus callosum. AJNR Am J Neuroradiol 23:803–808.

Cho KH, Yeh CH, Tournier JD, Chao YP, Chen JH, Lin CP (2008): Evaluation of the accuracy and angular resolution of q-ball imaging. Neuroimage 42:262–271.

Chung MK, Dalton KM, Alexander AL, Davidson RJ (2004): Less white matter concentration in autism: 2D voxel-based morphometry. Neuroimage 23:242–251.

Clarke JM, Zaidel E (1994): Anatomical–behavioral relationships: Corpus callosum morphometry and hemispheric specialization. Behav Brain Res 64(1/2):185–202.

Cook PA, Zhang H, Avants BB, Yushkevich P, Alexander DC, Gee JC, Ciccarelli O, Thompson AJ (2005): An automated approach to connectivity-based partitioning of brain structures. Med Image Comput Comput Assist Interv Int Conf Med Image Comput Comput Assist Interv 8 (Pt 1):164–171.

Descoteaux M, Angelino E, Fitzgibbons S, Deriche R (2007): Regularized, fast, and robust analytical Q-ball imaging. Magn Reson Med 58:497–510.

Descoteaux M, Deriche R, Knoesche T, Anwander A (2009): Deterministic and probabilistic tractography based on complex fiber orientation distributions. IEEE Trans Med Imaging 28:269–286.

Diwadkar VA, DeBellis MD, Sweeney JA, Pettegrew JW, Keshavan MS (2004): Abnormalities in MRI-measured signal intensity in the corpus callosum in schizophrenia. Schizophr Res 67(2/3):277–282.

Dougherty RF, Ben-Shachar M, Bammer R, Brewer AA, Wandell BA (2005): Functional organization of human occipital–callosal fiber tracts. Proc Natl Acad Sci USA 102:7350–7355.

Dougherty RF, Ben-Shachar M, Deutsch GK, Hernandez A, Fox GR, Wandell BA (2007): Temporal–callosal pathway diffusivity predicts phonological skills in children. Proc Natl Acad Sci USA 104:8556–8561.

Duara R, Kushch A, Gross-Glenn K, Barker WW, Jallad B, Pascal S, Loewenstein DA, Sheldon J, Rabin M, Levin B, Lubs H (1991): Neuroanatomic differences between dyslexic and normal readers on magnetic resonance imaging scans. Arch Neurol 48:410–416.

Friman O, Farneback G, Westin CF (2006): A Bayesian approach for stochastic white matter tractography. IEEE Trans Med Imaging 25:965.

Giedd JN, Castellanos FX, Casey BJ, Kozuch P, King AC, Hamburger SD, Rapoport JL (1994): Quantitative morphology of the corpus callosum in attention deficit hyperactivity disorder. Am J Psychiatry 151:665–669.

Hess CP, Mukherjee P, Han ET, Xu D, Vigneron DB (2006): Q-ball reconstruction of multimodal fiber orientations using the spherical harmonic basis. Magn Reson Med 56:104–117.

Hofer S, Frahm J (2006): Topography of the human corpus callosum revisited—Comprehensive fiber tractography using diffusion tensor magnetic resonance imaging. Neuroimage 32: 989–994.

Hua K, Zhang J, Wakana S, Jiang H, Li X, Reich DS, Calabresi PA, Pekar JJ, van Zijl PC, Mori S (2008): Tract probability maps in stereotaxic spaces: Analyses of white matter anatomy and tract-specific quantification. Neuroimage 39:336–347.

Huang H, Zhang J, van Zijl PC, Mori S (2004): Analysis of noise effects on DTI-based tractography using the brute-force and multi-ROI approach. Magn Reson Med 52:559–565.

Huang H, Zhang J, Jiang H, Wakana S, Poetscher L, Miller MI, van Zijl PC, Hillis AE, Wytik R, Mori S (2005): DTI tractography based parcellation of white matter: Application to the mid-sagittal morphology of corpus callosum. Neuroimage 26:195–205.

Hynd GW, Hall J, Novey ES, Eliopulos D, Black K, Gonzalez JJ, Edmonds JE, Riccio C, Cohen M (1995): Dyslexia and corpus callosum morphology. Arch Neurol 52:32–38.

Iturria-Medina Y, Canales-Rodriguez EJ, Melie-Garcia L, Valdes-Hernandez PA, Martinez-Montes E, Aleman-Gomez Y, Sanchez-Bornot JM (2007): Characterizing brain anatomical connections using diffusion weighted MRI and graph theory. Neuroimage 36:645–660.

Johansen-Berg H, Behrens TE, Sillery E, Ciccarelli O, Thompson AJ, Smith SM, Matthews PM (2005): Functional–anatomical validation and individual variation of diffusion tractography-based segmentation of the human thalamus. Cereb Cortex 15:31–39.

Jones DK, Pierpaoli C (2005): Confidence mapping in diffusion tensor magnetic resonance imaging tractography using a bootstrap approach. Magn Reson Med 53:1143–1149.

Jones DK, Griffin LD, Alexander DC, Catani M, Horsfield MA, Howard R, Williams SC (2002): Spatial normalization and averaging of diffusion tensor MRI data sets. Neuroimage 17:592–617.

Klein JC, Behrens TE, Robson MD, Mackay CE, Higham DJ, Johansen-Berg H (2007): Connectivity-based parcellation of human cortex using diffusion MRI: Establishing reproducibility, validity and observer independence in BA 44/45 and SMA/pre-SMA. Neuroimage 34:204–211.

Lazar M, Alexander AL (2005): Bootstrap white matter tractography (BOOT-TRAC). Neuroimage 24:524–532.

Luders E, Di Paola M, Tomaiuolo F, Thompson PM, Toga AW, Vicari S, Petrides M, Caltagirone C (2007): Callosal morphology in Williams syndrome: A new evaluation of shape and thickness. Neuroreport 18:203–207.

Makris N, Papadimitriou GM, Sorg S, Kennedy DN, Caviness VS, Pandya DN (2007): The occipitofrontal fascicle in humans: A quantitative, in vivo, DT-MRI study. Neuroimage 37:1100–1111.

Mazziotta JC, Toga AW, Evans A, Fox P, Lancaster J (1995): A probabilistic atlas of the human brain: Theory and rationale for its development. The International Consortium for Brain Mapping (ICBM). Neuroimage 2:89–101.

Meyer BU, Roricht S, Woiciechowsky C (1998): Topography of fibers in the human corpus callosum mediating interhemispheric inhibition between the motor cortices. Ann Neurol 43:360–369.

Ming-Chang C, Leow AD, Klunder AD, Dutton RA, Barysheva M, Rose SE, McMahon KL, de Zubicaray GI, Toga AW, Thompson PM (2008): Fluid registration of diffusion tensor images using information theory. IEEE Trans Med Imaging 27:442–456.

Miyata J, Hirao K, Namiki C, Fukuyama H, Okada T, Miki Y, Hayashi T, Murai T (2007): Interfrontal commissural abnormality in schizophrenia: Tractography-assisted callosal parcellation. Schizophr Res 97(1–3):236–241.

Mori S, van Zijl PC (2002): Fiber tracking: Principles and strategies—A technical review. NMR Biomed 15(7/8):468–480.

Morris DM, Embleton KV, Parker GJ (2008): Probabilistic fibre tracking: Differentiation of connections from chance events. Neuroimage 42:1329–1339.

Muetzel RL, Collins PF, Mueller BA, A MS, Lim KO, Luciana M (2008): The development of corpus callosum microstructure and associations with bimanual task performance in healthy adolescents. Neuroimage 39:1918–1925.

Narr KL, Thompson PM, Sharma T, Moussai J, Cannestra AF, Toga AW (2000): Mapping morphology of the corpus callosum in schizophrenia. Cereb Cortex 10:40–49.

Narr KL, Cannon TD, Woods RP, Thompson PM, Kim S, Asunction D, van Erp TG, Poutanen VP, Huttunen M, Lönnqvist J, Standerksjöld-Nordenstam CG, Kaprio J, Mazziotta JC, Toga AW (2002): Genetic contributions to altered callosal morphology in schizophrenia. J Neurosci 22:3720–3729.

Ozarslan E, Shepherd TM, Vemuri BC, Blackband SJ, Mareci TH (2006): Resolution of complex tissue microarchitecture using the diffusion orientation transform (DOT). Neuroimage 31:1086–1103.

Park HJ, Kubicki M, Shenton ME, Guimond A, McCarley RW, Maier SE, Kikinis R, Jolesz FA, Westin CF (2003): Spatial normalization of diffusion tensor MRI using multiple channels. Neuroimage 20:1995–2009.

Park HJ, Kim JJ, Lee SK, Seok JH, Chun J, Kim DI, Lee JD (2008): Corpus callosal connection mapping using cortical gray matter parcellation and DT-MRI. Hum Brain Mapp 29:503–516.

Parker GJ, Alexander DC (2005): Probabilistic anatomical connectivity derived from the microscopic persistent angular structure of cerebral tissue. Philos Trans R Soc Lond B Biol Sci 360:893–902.

Parker GJ, Haroon HA, Wheeler-Kingshott CA (2003): A framework for a streamline-based probabilistic index of connectivity (PICo) using a structural interpretation of MRI diffusion measurements. J Magn Reson Imaging 18:242–254.

Petrides M, Pandya DN (1988): Association fiber pathways to the frontal cortex from the superior temporal region in the rhesus monkey. J Comp Neurol 273:52–66.

Pichon E, Westin CF, Tannenbaum AR (2005): A Hamilton–Jacobi–Bellman approach to high angular resolution diffusion tractography. Med Image Comput Comput Assist Interv Int Conf Med Image Comput Comput Assist Interv 8 (Pt 1):180–187.

Rajapakse JC, Giedd JN, Rumsey JM, Vaituzis AC, Hamburger SD, Rapoport JL (1996): Regional MRI measurements of the corpus callosum: A methodological and developmental study. Brain Dev 18:379–388.

Randall PL (1983): Schizophrenia, abnormal connection, and brain evolution. Med Hypotheses 10:247–280.

Rotarska-Jagiela A, Schonmeyer R, Oertel V, Haenschel C, Vogeley K, Linden DE (2008): The corpus callosum in schizophrenia-volume and connectivity changes affect specific regions. Neuroimage 39:1522–1532.

Savadjiev P, Campbell JS, Pike GB, Siddiqi K (2006): 3D curve inference for diffusion MRI regularization and fibre tractography. Med Image Anal 10:799–813.

Savadjiev P, Campbell JS, Descoteaux M, Deriche R, Pike GB, Siddiqi K (2008): Labeling of ambiguous subvoxel fibre bundle configurations in high angular resolution diffusion MRI. Neuroimage 41:58–68.

Semrud-Clikeman M, Filipek PA, Biederman J, Steingard R, Kennedy D, Renshaw P, Bekken K (1994): Attention-deficit hyperactivity disorder: magnetic resonance imaging morphometric analysis of the corpus callosum. J Am Acad Child Adolesc Psychiatry 33:875–881.

Skranes J, Vangberg TR, Kulseng S, Indredavik MS, Evensen KA, Martinussen M, Dale AM, Haraldseth O, Brubakk AM (2007): Clinical findings and white matter abnormalities seen on diffusion tensor imaging in adolescents with very low birth weight. Brain 130 (Pt 3):654–666.

Stievenart JL, Iba-Zizen MT, Tourbah A, Lopez A, Thibierge M, Abanou A, Cabanis EA (1997): Minimal surface: A useful paradigm to describe the deeper part of the corpus callosum? Brain Res Bull 44:117–124.

Styner MA, Oguz I, Smith RG, Cascio C, Jomier M (2005): Corpus callosum subdivision based on a probabilistic model of interhemispheric connectivity. Med Image Comput Comput Assist Interv Int Conf Med Image Comput Comput Assist Interv 8 (Pt 2):765–772.

Thottakara P, Lazar M, Johnson SC, Alexander AL (2006): Application of Brodmann's area templates for ROI selection in white matter tractography studies. Neuroimage 29:868–878.

Tomaiuolo F, Di Paola M, Caravale B, Vicari S, Petrides M, Caltagirone C (2002): Morphology and morphometry of the corpus callosum in Williams syndrome: A T1-weighted MRI study. Neuroreport 13:2281–2284.

Tournier JD, Calamante F, Gadian DG, Connelly A (2004): Direct estimation of the fiber orientation density function from diffusion-weighted MRI data using spherical deconvolution. Neuroimage 23:1176–1185.

Tournier JD, Calamante F, Connelly A (2007): Robust determination of the fibre orientation distribution in diffusion MRI: Non-negativity constrained super-resolved spherical deconvolution. Neuroimage 35:1459–1472.

Tuch DS (2004): Q-ball imaging. Magn Reson Med 52:1358–1372.

Tuch DS, Reese TG, Wiegell MR, Makris N, Belliveau JW, Wedeen VJ (2002): High angular resolution diffusion imaging reveals intravoxel white matter fiber heterogeneity. Magn Reson Med 48:577–582.

Tuch DS, Reese TG, Wiegell MR, Wedeen VJ (2003): Diffusion MRI of complex neural architecture. Neuron 40:885–895.

Vogt BA, Pandya DN (1978): Cortico-cortical connections of somatic sensory cortex (areas 3, 1 and 2) in the rhesus monkey. J Comp Neurol 177:179–191.

Wahl M, Lauterbach-Soon B, Hattingen E, Jung P, Singer O, Volz S, Klein JC, Steinmetz H, Ziemann U (2007): Human motor corpus callosum: Topography, somatotopy, and link between microstructure and function. J Neurosci 27:12132–12138.

Wakana S, Jiang H, Nagae-Poetscher LM, van Zijl PC, Mori S (2004): Fiber tract-based atlas of human white matter anatomy. Radiology 230:77–87.

Wedeen VJ, Hagmann P, Tseng WY, Reese TG, Weisskoff RM (2005): Mapping complex tissue architecture with diffusion spectrum magnetic resonance imaging. Magn Reson Med 54:1377–1386.

Weis S, Kimbacher M, Wenger E, Neuhold A (1993): Morphometric analysis of the corpus callosum using MR: correlation of measurements with aging in healthy individuals. AJNR Am J Neuroradiol 14:637–645.

Westerhausen R, Kreuder F, Dos Santos Sequeira S, Walter C, Woerner W, Wittling RA, Schweiger E, Wittling W (2004): Effects of handedness and gender on macro- and microstructure of the corpus callosum and its subregions: A combined high-resolution and diffusion-tensor MRI study. Brain Res Cogn Brain Res 21:418–426.

Witelson SF (1989): Hand and sex differences in the isthmus and genu of the human corpus callosum. A postmortem morphological study. Brain 112 (Pt 3):799–835.

Xu D, Mori S, Solaiyappan M, van Zijl PC, Davatzikos C (2002): A framework for callosal fiber distribution analysis. Neuroimage 17:1131–1143.

Xu D, Mori S, Shen D, van Zijl PC, Davatzikos C (2003): Spatial normalization of diffusion tensor fields. Magn Reson Med 50:175–182.

Zarei M, Johansen-Berg H, Smith S, Ciccarelli O, Thompson AJ, Matthews PM (2006): Functional anatomy of interhemispheric cortical connections in the human brain. J Anat 209:311–320.

Zarei M, Johansen-Berg H, Jenkinson M, Ciccarelli O, Thompson AJ, Matthews PM (2007): Two-dimensional population map of cortical connections in the human internal capsule. J Magn Reson Imaging 25:48–54.

Zhang F, Hancock ER, Goodlett C, Gerig G (2009): Probabilistic white matter fiber tracking using particle filtering and von Mises–Fisher sampling. Med Image Anal 13:5–18.

Zhang H, Yushkevich PA, Alexander DC, Gee JC (2006): Deformable registration of diffusion tensor MR images with explicit orientation optimization. Med Image Anal 10:764–785.

APPENDIX

Neural connections derived by QBI with MFACT algorithm may propagate from a single voxel within the CC to plenty of terminations, which is unlike to the results from DTI-based streamline tractography. To reveal the connection probability, the number of tract terminations located in each BA from individual CC voxel was calculated. The primary and secondary dominant BAs were thus defined by the numbers of tract terminations, i.e. the most and the secondary connections from each voxel.

To evaluate reliability of the most dominant connection map, the voxel-by-voxel correspondence map between individual primary connections was calculated by Eq. 2. The voxel-by-voxel correspondence rate of primary dominant connection was defined as follows:

$$H_1(v,b) = \sum_{s=0}^{S} \sum_{b=1}^{52} \delta(b - d_1(s,v)), \tag{2}$$

where $\delta(x) = 1$, for $x = 0$; $\delta(x) = 0$, for $x \neq 0$

$$C_1(v) = \frac{1}{S} \arg \max_b \{H_1(v,b)\}, \quad b \in \{1,2,\ldots,52\}$$

where $d_1(s, v)$ was the label of the primary dominant BA at the voxel v of a single subject. $H_1(v, b)$ was regarded as the primary dominant BA histogram of all subjects at the voxel v. Among the 52 BAs, 28 BA subregions were selected for parcellation of the CC. The correspondence rate $C_1(v)$ for primary dominant BA at the voxel v was the ratio of the maximum value of primary BAs histogram versus the number of subjects. Similarly, the voxel-by-voxel correspondence rate of secondary dominant connection was defined as follows:

$$H_2(v,b) = \sum_{s=0}^{S} \sum_{b=1}^{52} \delta(b - d_2(s,v)), \tag{3}$$

where $\delta(x) = 1$, for $x = 0$; $\delta(x) = 0$, for $x \neq 0$

$$C_2(v) = \frac{1}{S} \arg \max_b \{H_2(v,b)\}, \quad b \in \{1,2,\ldots,52\}$$

where $d_2(s, v)$ was the label of the secondary dominant BA at the voxel v of a single subject. $H_2(v, b)$ was regarded as the secondary dominant BA histogram of all subjects at the voxel v.

Besides, to take the primary and secondary primary BA indices into account simultaneously at each CC voxel, additional correspondence rate was defined as follows:

$$H_{1\&2}(v,b) = \sum_{s=0}^{S} \sum_{b=1}^{52} \{\delta(b - d_1(s,v)) + \delta(b - d_2(s,v))\}, \tag{4}$$

where $\delta(x) = 1$, for $x = 0$; $\delta(x) = 0$, for $x \neq 0$

$$C_{1\&2}(v) = \frac{1}{S} \arg \max_b \{H_{1\&2}(v,b)\}, \quad b \in \{1,2,\ldots,52\}$$

The correspondence rate of first and second most primary connection map $C_{1\&2}(v)$ was calculated accordingly (Eq. 4).